

Ground state correlations in ^{16}O and ^{40}Ca A. Fabrocini,¹ F. Arias de Saavedra,² and G. Co³¹*Dipartimento di Fisica, Università di Pisa, and Istituto Nazionale di Fisica Nucleare, sezione di Pisa, I-56100 Pisa, Italy*²*Departamento de Física Moderna, Universidad de Granada, E-18071 Granada, Spain*³*Dipartimento di Fisica, Università di Lecce and Istituto Nazionale di Fisica Nucleare, sezione di Lecce, I-73100 Lecce, Italy*

(Received 14 October 1999; published 24 February 2000)

We study the ground state properties of doubly closed shell nuclei ^{16}O and ^{40}Ca in the framework of correlated basis function theory using state dependent correlations, with central and tensor components. The realistic Argonne v_{14} and v'_8 two-nucleon potentials and three-nucleon potentials of the Urbana class have been adopted. By means of the Fermi hypernetted chain integral equations, in conjunction with the single operator chain approximation, we evaluate the ground state energy, one- and two-body densities and electromagnetic and spin static responses for both nuclei. In ^{16}O we compare our results with the available Monte Carlo and coupled cluster ones and find a satisfying agreement. As in the nuclear matter case with similar interactions and wave functions, the nuclei result underbound by 2–3 MeV/nucleon.

PACS number(s): 21.60.Gx, 21.10.Dr, 27.20.+n, 27.40.+z

I. INTRODUCTION

The attempt to describe all nuclei starting from the same nucleon-nucleon interaction which reproduces the properties of two-, and possibly three-, nucleon systems is slowly obtaining its first successes. A set of techniques to exactly solve the Schrödinger equation in the $3 \leq A \leq 8$ nuclei is now available: Faddeev [1], correlated hyperspherical harmonics expansion [2], quantum Monte Carlo [3]. Their straightforward extension to medium-heavy nuclei is however not yet feasible, both for computational and theoretical reasons.

The correlated basis function (CBF) theory is one of the most promising many-body tools currently under development to attack the problem of dealing with the complicated structure (short range repulsion and strong state dependence) of the nuclear interaction. The CBF has a long record of applications in condensed matter physics, as well as in liquid helium and electron systems. In nuclear physics the most extensive use of CBF has been done in infinite nuclear and neutron matter. The neutron stars structure described via the CBF based neutron matter equation of state is in nice agreement with the current observational data [4,5]. In nuclear matter CBF has been used not only to study ground state properties [4,6,7] but also dynamical quantities, as electromagnetic responses [8,9] and one-body Green's functions [10].

The CBF theory is based upon the variational principle, i.e., one searches for the minimum of the energy functional

$$E[\Psi] = \frac{\langle \Psi | H | \Psi \rangle}{\langle \Psi | \Psi \rangle} \quad (1)$$

in the Hilbert subspace of the correlated many-body wave functions Ψ :

$$\Psi(1,2\dots A) = G(1,2\dots A)\Phi(1,2\dots A), \quad (2)$$

where $G(1,2\dots A)$ is a many-body correlation operator acting on the mean field wave function $\Phi(1,2\dots A)$ [we will take a Slater determinant of single particle wave functions, $\phi_\alpha(i)$].

In realistic nuclear matter calculations, the correlation operator is given by a symmetrized product of two-body correlation operators F_{ij} :

$$G(1,2\dots A) = S \left[\prod_{i < j} F_{ij} \right]. \quad (3)$$

In principle richer choices for the operator (3) can be made by including explicit three- or more-nucleon correlations, which cannot be described by the product of two-body correlations. It is essential, however, that the two-body correlation F_{ij} has an operatorial dependence analogous to that of the modern nucleon-nucleon interactions [11–15]. Nowadays, sophisticated CBF calculations consider F_{ij} of the form

$$F_{ij} = \sum_{p=1,8} f^p(r_{ij}) O_{ij}^p, \quad (4)$$

where the involved operators are

$$O_{ij}^{p=1,8} = [1, \boldsymbol{\sigma}_i \cdot \boldsymbol{\sigma}_j, S_{ij}, (\mathbf{L} \cdot \mathbf{S})_{ij}] \otimes [1, \boldsymbol{\tau}_i \cdot \boldsymbol{\tau}_j] \quad (5)$$

and $S_{ij} = (3 \hat{\mathbf{r}}_{ij} \cdot \boldsymbol{\sigma}_i \hat{\mathbf{r}}_{ij} \cdot \boldsymbol{\sigma}_j - \boldsymbol{\sigma}_i \cdot \boldsymbol{\sigma}_j)$ is the tensor operator. The correlation functions $f^p(r)$, as well as the set of single particle wave functions, are fixed by the energy minimization procedure.

A key point in applying CBF is the evaluation of the many-variables integrals necessary to calculate the energy functional (1). A direct approach consists in using Monte Carlo sampling techniques (variational Monte Carlo, VMC) [16]. However, the required numerical effort is such that, for realistic interactions and correlations, VMC can be efficiently used only in light nuclei. Actually, a realistic calculation of the ground state of ^{16}O has been done in Ref. [17] by using the so called cluster Monte Carlo (CMC) method. In CMC the terms related to the scalar part of the correlation ($p=1$) are completely summed by VMC, whereas the remaining operatorial ($p>1$) contributions are approximated by considering up to four- or five-body cluster terms.

An alternative to the Monte Carlo methodology is provided by cluster expansions and the integral summation technique known as Fermi hypernetted chain (FHNC) [18], particularly suited to treat heavy systems. By means of the FHNC equations it is possible to sum infinite classes of Mayer-like diagrams resulting from the cluster expansion of the expectation value of the Hamiltonian, or of any other operator. FHNC has been widely applied to both finite and infinite systems with purely scalar (state independent, or Jastrow) correlations.

The case of the state dependent F_{ij} , needed in nuclear systems, is more troublesome since the noncommutativity of the correlation operators prevents the development of a complete FHNC theory for the correlated wave function of Eq. (2). For this reason an approximated treatment of the operatorial correlations, called single operator chain (SOC), has been developed [19]. The SOC approximation, together with a full FHNC treatment of the Jastrow part of the correlation, provides an accurate description of infinite nucleonic matter [4]. It is therefore believed that FHNC/SOC effectively includes the contribution of many-body correlated clusters at all orders. The evaluation of additional classes of diagrams in nuclear matter has set the estimated accuracy for the ground state energy to less than 1 MeV at saturation density ($\rho_{nm}=0.16 \text{ fm}^{-3}$) [4,20].

In a series of papers [21–23] we have extended the FHNC scheme to describe the ground state of doubly closed shell nuclei, from ${}^4\text{He}$ to ${}^{208}\text{Pb}$, with semirealistic, central interactions and two-body correlations, either of the Jastrow type or depending, at most, on the third components of the isospins of the correlated nucleons. In Ref. [24] we used FHNC/SOC to evaluate energies and densities of the ${}^{16}\text{O}$ and ${}^{40}\text{Ca}$ nuclei, having doubly closed shells in the ls coupling scheme, with potentials and correlations containing operator terms up to the tensor components. In the ${}^{16}\text{O}$ nucleus the comparison of our results with those of a CMC calculation confirmed the accuracy of the FHNC/SOC approximation estimated in nuclear matter.

The present work is the extension of that of Ref. [24]. The ground state properties of the ${}^{16}\text{O}$ and ${}^{40}\text{Ca}$ nuclei are calculated within the FHNC/SOC formalism by using a complete, realistic nucleon-nucleon potential, with $p > 6$ components, and by considering also three-nucleon interactions. The two-nucleon interactions we have employed are the Argonne v_{14} [25] potential and the v'_8 reduction of the Argonne v_{18} [14] potential. For the three-nucleon interaction we have adopted the Urbana models, Urbana VII [26] with Argonne v_{14} and Urbana IX [3] with Argonne v'_8 . In addition to the energy and the densities, we have also evaluated the static responses. They are the nonenergy weighted sums of the inclusive dynamical responses of the nucleus to external probes. We have studied the density, the electromagnetic, and the spin static responses, both in the longitudinal and transverse channels.

The paper is organized as follows: in Sec. II we briefly present the interaction and the correlated wave function properties and recall the basic features of FHNC/SOC; Sec. III deals in short with the insertion of the spin-orbit components and of the three-nucleon potential; in Sec. IV we show

and discuss the results for the energy, one- and two-body densities and static responses; the conclusions are drawn in Sec. V.

II. INTERACTION, CORRELATED WAVE FUNCTION, AND CLUSTER EXPANSION

We work in the framework of the nonrelativistic description of the nucleus and use a Hamiltonian of the form

$$H = \frac{-\hbar^2}{2m} \sum_i \nabla_i^2 + \sum_{i<j} v_{ij} + \sum_{i<j<k} v_{ijk}. \quad (6)$$

Very high quality phase-shift analyses of a large body of pp and np data have been recently carried out [11,12]. Building on this accurate data base, several nucleon-nucleon (NN) potentials have been constructed, like the updated Nijmegen interaction [13], the CD Bonn interaction [15] and the Argonne v_{18} (A18) [14] interaction. All of them include charge symmetry breaking terms in order to provide a precise fit to both the pp and np data.

The structure of v_{ij} and v_{ijk} , at large interparticle distances is dictated by meson exchange processes. The long-range part of the NN interactions is determined by the one-pion exchange (OPE):

$$v_{ij}^{OPE} = \frac{f_{\pi NN}^2}{4\pi} \frac{m_\pi}{3} [Y_\pi(r_{ij}) \boldsymbol{\sigma}_i \cdot \boldsymbol{\sigma}_j + T_\pi(r_{ij}) S_{ij}] \boldsymbol{\tau}_i \cdot \boldsymbol{\tau}_j, \quad (7)$$

where m_π is the pion mass (138.03 MeV), ($f_{\pi NN}^2/4\pi$) = 0.081, and $Y_\pi(r)$ and $T_\pi(r)$ are the Yukawa and tensor Yukawa functions,

$$Y_\pi(r) = \frac{e^{-\mu r}}{\mu r}, \quad (8)$$

$$T_\pi(r) = \frac{e^{-\mu r}}{\mu r} \left[1 + \frac{3}{\mu r} + \frac{3}{(\mu r)^2} \right], \quad (9)$$

with $\mu \sim 0.7 \text{ fm}^{-1}$. The Argonne potentials simulate the effects of ρ exchange, not explicitly included [25], by modifying the Yukawa functions with a short-range cutoff, $Y_\pi(r) \rightarrow Y(r) = Y_\pi(r) F_{cut}(r)$ and $T_\pi(r) \rightarrow T(r) = T_\pi(r) F_{cut}^2(r)$ with $F_{cut}(r) = 1 - \exp(-cr^2)$ ($c = 2 \text{ fm}^{-2}$). The intermediate and short-range parts of this class of potentials are mostly phenomenological and A18 is parametrized according to the operatorial structure

$$v_{ij} = \sum_{p=1,18} v^p(r_{ij}) O_{ij}^p, \quad (10)$$

where the first 14 components,

$$O_{ij}^{p=1,14} = [1, \boldsymbol{\sigma}_i \cdot \boldsymbol{\sigma}_j, S_{ij}, (\mathbf{L} \cdot \mathbf{S})_{ij}, L^2, L^2 \boldsymbol{\sigma}_i \cdot \boldsymbol{\sigma}_j, (\mathbf{L} \cdot \mathbf{S})_{ij}^2] \\ \otimes [1, \boldsymbol{\tau}_i \cdot \boldsymbol{\tau}_j], \quad (11)$$

give the isoscalar part, defining a v_{14} -like potential (A14),

$$v_{14,ij} = \sum_{p=1,14} v^p(r_{ij}) O_{ij}^p. \quad (12)$$

The remaining four components of A_{18} are of the isovector ($\tau_{i,z} + \tau_{j,z}$) and isotensor ($3\tau_{i,z}\tau_{j,z} - \tau_i \cdot \tau_j$) type. The Argonne v_8' potential ($A_{8'}$) is an eight operators reduction of A_{18} built to reproduce the isoscalar part of the full interaction in the S , P , and 3D_1 waves and the ${}^3D_1 - {}^3S_1$ coupling [3].

Other potentials use different parametrizations. For instance, the Nijmegen model [12] employs \mathbf{p}^2 operators instead of \mathbf{L}^2 .

The longest range part of the three-nucleon interactions (TNI) involves a two pions exchange with the intermediate excitation of a Δ [27]:

$$v_{ijk}^{2\pi} = A_{2\pi} \sum_{cyc} \left(\{X_{ij}, X_{ik}\} \{ \boldsymbol{\tau}_i \cdot \boldsymbol{\tau}_j, \boldsymbol{\tau}_i \cdot \boldsymbol{\tau}_k \} + \frac{1}{4} [X_{ij}, X_{ik}] \right. \\ \left. \times [\boldsymbol{\tau}_i \cdot \boldsymbol{\tau}_j, \boldsymbol{\tau}_i \cdot \boldsymbol{\tau}_k] \right), \quad (13)$$

where

$$X_{ij} = Y(r_{ij}) \boldsymbol{\sigma}_i \cdot \boldsymbol{\sigma}_j + T(r_{ij}) S_{ij}, \quad (14)$$

and the symbols $[,]$ and $\{, \}$ indicate the commutator and anticommutator operators, respectively.

The Urbana class of TNI [28] introduces an additional, repulsive, spin, and isospin independent, short range term,

$$v_{ijk}^R = U_0 \sum_{cyc} T^2(r_{ij}) T^2(r_{ik}), \quad (15)$$

which simulates dispersive effects when integrating out Δ degrees of freedom. The total Urbana TNI are then given by the sum of the two terms defined above, $v_{ijk} = v_{ijk}^{2\pi} + v_{ijk}^R$, and the $A_{2\pi}$ and U_0 parameters are adjusted to provide a good fit to the binding energies of few-body nuclei and nuclear matter. In the A_{14} +Urbana VII (A_{14} +UVII) model the values $A_{2\pi} = -0.0333$ MeV and $U_0 = 0.0038$ MeV have been fixed by variational calculations. In the most recent A_{18} +Urbana IX (A_{18} +UIX) model the values $A_{2\pi} = -0.0293$ MeV and $U_0 = 0.0048$ MeV have been obtained with a quantum Monte Carlo calculation for ${}^3\text{H}$ and a variational calculation for nuclear matter. The values of $A_{2\pi}$ are in good agreement with those predicted by the pure two-pions exchange model ($A_{2\pi} \sim -0.03$ MeV).

The truncated $A_{8'}$ NN potential was introduced in Ref. [3] because its simpler parametrization allowed a simplification of the numerically involved quantum Monte Carlo calculations. The contribution of the missing channels was perturbatively evaluated. One should remark, however, that $A_{8'}$ was found to give a slight overbind. For this reason, the strength of the repulsive part of the TNI Urbana IX model was increased by $\sim 30\%$ to reproduce the experimental energies. The results presented in this paper have been obtained with the A_{14} +UVII and $A_{8'}$ +UIX models, where the Urbana IX interaction has been redefined as above.

The many-body wave function (2) contains two ingredients: the correlation functions $f^p(r)$ and the single particle states forming the Slater determinant $\Phi(1,2,\dots,A)$. In our calculations we have used a f_6 -type correlation, so neglecting the spin-orbit components. This choice will be discussed and commented on later in the paper.

The best variational choice of F_{ij} would be given by the free minimization of the FHNC/SOC energy and the solution of the corresponding Euler equations, $\delta E / \delta F_{ij} = 0$. This approach is not practicable in finite nuclear systems, so we use an effective correlation obtained by the minimization of the energy evaluated at the lowest order of the cluster expansion E_{LO} . The two-body Euler equations are then solved under the healing conditions $f^1(r \geq d_1) = 1$, $f^{p>1}(r \geq d_p) = 0$ and requiring that the first derivatives of these functions at $r = d_p$ vanish. The healing distances d_p are taken as variational parameters. In analogy with the nuclear matter case, in our calculations we adopt only two healing distances: d_c for the four central channels and d_t for the two tensor ones. Additional variational parameters are the quenching factors α^p of the NN potentials in the Euler equations. More details are given in Ref. [19] for nuclear matter and in Ref. [24] for finite nuclei. In the CMC calculation of Ref. [17] a nuclear matter Euler correlation was used and the nuclear matter Fermi momentum k_F was used as a variational parameter. We follow here the same strategy.

The single particle wave functions $\phi_\alpha(i)$ used in this work have been obtained either by solving the single particle Schrödinger equation with Woods-Saxon potential,

$$V_{ws}(r) = \frac{V_0}{1 + \exp[(r - R_0)/a_0]}, \quad (16)$$

or with a harmonic oscillator well $V_{HO}(r)$ with oscillator length $b_{HO} = \sqrt{\hbar/m\omega}$. The parameters V_0 , R_0 , and a_0 of $V_{ws}(r)$ and b_{HO} of $V_{HO}(r)$ are also variationally determined.

It is possible to express the expectation values of n -body operators in terms of n -body density matrices, and related quantities. In particular, the one- and two-body densities, $\rho_1(\mathbf{r}_1)$ and $\rho_2^p(\mathbf{r}_1, \mathbf{r}_2)$, defined as

$$\rho_1(\mathbf{r}) = \left\langle \sum_i \delta(\mathbf{r} - \mathbf{r}_i) \right\rangle \quad (17)$$

and

$$\rho_2^p(\mathbf{r}, \mathbf{r}') = \left\langle \sum_{i \neq j} \delta(\mathbf{r} - \mathbf{r}_i) \delta(\mathbf{r}' - \mathbf{r}_j) O_{ij}^p \right\rangle, \quad (18)$$

are needed to compute the energy mean value (1). In the above expressions we indicate the mean value of an operator Q as $\langle Q \rangle = \langle \Psi | Q | \Psi \rangle / \langle \Psi | \Psi \rangle$. Cluster expansion and Fermi hypernetted chain theory provide a viable way to evaluate the densities both in infinite and finite Fermi systems. We present here only some of the basic features of the FHNC/SOC computational scheme. More complete discussions of

the FHNC theory are found in Refs. [18] and [21] for scalar correlations and in Refs. [19] and [24] for the operatorial case.

In FHNC theory, with scalar correlations, the densities are written in terms of the correlation $f^1(r)$ and of the *nodal* and *elementary* functions $N_{xy}^1(\mathbf{r}_1, \mathbf{r}_2)$ and $E_{xy}^1(\mathbf{r}_1, \mathbf{r}_2)$, representing the sums of the corresponding nodal and elementary cluster diagrams. The $x(y)$ label characterizes the exchange pattern at the external points 1(2) and can indicate: a direct link (d) if the particle is not exchanged and the point is reached by a dynamical correlation, $h(r)=[f^1(r)]^2-1$; an exchange link (e) if the particle belongs to a closed exchange loop; a cyclic link (c) if the particle belongs to an open exchange loop. The possible combinations are: dd , de , ed , ee , and cc . In infinite, homogeneous systems, as nuclear matter, the FHNC functions depend only on the interparticle distance r_{12} . The FHNC integral equations allow for computing the nodal functions, once the elementary ones are known.

With the introduction of operatorial correlations, the nodal functions gain a state dependence, $N_{xy}^{p \geq 1}(\mathbf{r}_1, \mathbf{r}_2)$. The correlation operators do not commute anymore among themselves, $[F_{12}, F_{13}] \neq 0$, and one must take into account the various possible orderings in Eq. (3). For this reason a complete FHNC treatment for the full, state dependent densities is, at present, not possible. The single operator chain approximation was introduced in Ref. [19] for nuclear matter, and extended to ls doubly closed shell nuclei in Ref. [24], for f_6 correlations. The SOC scheme consists in summing those $p > 1$ chains, where each link may contain only one operatorial element and scalar dressings at all orders. Notice that operatorial dependence comes also on account of the exchanges of two or more nucleons, since the space exchange operator is given by $P_{ij} = -\sum_{p=c,\sigma,\tau,\sigma\tau} O_{ij}^p/4$. Here, and in the following, we may refer to the operatorial channels as c ($p=1$), σ (spin), t (tensor), and b (spin orbit). The isospin channels have an extra τ label.

The elementary functions $E_{xy}(\mathbf{r}_1, \mathbf{r}_2)$ represent an input to the FHNC equations, as they cannot be calculated in a closed form. The FHNC/0 approximation consists in neglecting all the elementary contributions. This seemingly crude approximation is actually based on the fact that the elementary diagrams are highly connected and have, at least, a quadratic dependence on the density of the system. These diagrams are not expected to produce relevant contributions in the relatively low density nuclear systems, whereas they are important in denser systems, like atomic liquid helium. A test of the validity of the FHNC/0 approximation, and, in general, of the importance of the elementary diagrams, is provided by the degree of accuracy in satisfying the densities normalizations. In Ref. [24] particular attention has been paid to the normalization of the one-body density,

$$A = \int d^3r_1 \rho_1(\mathbf{r}_1), \quad (19)$$

and to that of the central and isospin two-body densities,

$$1 = \frac{1}{A(A-1)} \int d^3r_1 \int d^3r_2 \rho_2^c(\mathbf{r}_1, \mathbf{r}_2), \quad (20)$$

$$-1 = \frac{1}{3A} \int d^3r_1 \int d^3r_2 \rho_2^{\bar{c}}(\mathbf{r}_1, \mathbf{r}_2). \quad (21)$$

Deviations of the sum rules from their exact values are due to (i) the approximate evaluation of the elementary diagrams and (ii) the SOC approximation. The first item has been already investigated in Ref. [21], where it has been found that the most relevant corrections to the FHNC/0 sum rules come from the E_{ee}^{exch} diagrams, i.e., ee -elementary diagrams whose external points belong to the same exchange loop. These diagrams mainly contribute to the isospin saturation sum rule (21) and to the potential energy, if the interaction has large exchange terms. This is understood if we notice that a four-point elementary diagram, linear in the central link $h(r)$, belongs to E_{ee}^{exch} , as well as diagrams linear in the operatorial link, $f^1(r)f^{p>1}(r)$.

In Ref. [24] it has been shown that the one-body density sum rule is violated in FHNC/SOC by less than 1% and the two-body density normalizations (20) and (21) by $\sim 9\%$ in the worst case (^{40}Ca with tensor correlations). This is the same degree of accuracy found in Ref. [4] for nuclear matter calculations.

In Ref. [24] the comparison of the ^{16}O FHNC energies calculated for a purely Jastrow correlation with the exact VMC estimates shows an excellent agreement, with a difference of $\sim 1\%$ in the kinetic energy (24.61 MeV in FHNC vs 24.33 ± 0.21 in VMC) and of $\sim 2\%$ in the potential energy (-22.07 MeV in FHNC vs -21.56 ± 0.25 in VMC). The ^{16}O FHNC energies calculated with a f_6 correlation and using the v_6 truncation of the Urbana v_{14} potential [29], have been compared with the results of a fifth order CMC calculation, which appeared to have reached a satisfying convergence. In this case we found a difference of less than 5% for the kinetic energy (31.16 MeV in FHNC/SOC vs 29.45 ± 0.33 in CMC) and of $\sim 7\%$ for the potential one (-35.47 MeV in FHNC/SOC vs -33.03 ± 0.31 in CMC). The FHNC/SOC calculation gives a binding energy per nucleon of -4.33 MeV to be compared with the -4.59 ± 0.10 MeV value obtained by CMC. This difference is compatible with the nuclear matter estimates.

III. SPIN-ORBIT AND THREE-BODY FORCES

As already mentioned in the Introduction, the novelty of this work with respect to Ref. [24] is the inclusion of the spin-orbit and three-body terms of the potential. In this section we briefly show how to extend the FHNC/SOC formalism to consider these parts of the interaction.

A. Spin-orbit potential

The treatment of the spin-orbit interaction within the FHNC/SOC formalism has been discussed in detail in Ref. [30] for the nuclear matter case. In that paper, the evaluation of the mean value of the spin-orbit terms of the interaction,

$\langle v^{7=b,8=b\tau} \rangle$, was done using a f_8 correlation factor, so including all the eight operatorial components in Eq. (4).

Here we extend the nuclear matter formalism to the finite nuclei case for a f_6 correlation. A correlation containing spin-orbit components would, probably, be more efficient from the variational point of view. However, these correlation terms introduce extra uncertainties in the cluster expansion, and we have chosen to work with a simpler correlation in favor of a safer convergence. We shall discuss further this point and give some estimates of the $f^{p>6}$ corrections.

In the FHNC/SOC scheme, the ground state matrix element W of a generic two-body operator \hat{W} is split into four parts:

$$W = W_0 + W_s + W_c + W_{cs}, \quad (22)$$

where W_0 indicates the sum of the diagrams with central chains between the fully correlated interacting points, connected by \hat{W} , W_s the sum of the diagrams having operatorial vertex corrections (or single operator rings) touching the interacting points and central chains, W_c the diagrams with one operatorial chain, SOC, between the interacting points, and, finally, W_{cs} the diagrams containing both operatorial vertex corrections and chains. A more complete discussion on this topic is found in Refs. [19] and [24].

The nuclear matter calculations of Ref. [30] show that two-body clusters provide the leading contribution to $\langle v^{b,b\tau} \rangle$. Three body separable diagrams, contributing to W_s , gave the main many-body contributions and were of the order of 10% of the two-body ones. Chain contributions were even smaller. These results have been confirmed in Ref. [7], where the authors found $\langle v^{b+b\tau} \rangle_{\text{two-body}}/A = -2.29$ MeV and a many-body contribution ($W_s + W_c$) of -0.28 MeV at the nuclear matter saturation density, with the $A18$ potential.

Relying on these facts, for the spin-orbit terms of the interaction, we have calculated only the W_0 contribution of Eq. (22) with a f_6 correlation function. It turns out that, in this case, only the tensor correlations contribute, and the full expression reads

$$\begin{aligned} \langle v^{bj\tau} \rangle_{W_0} = & -9 \int d^3 r_1 \int d^3 r_2 f^{ti\tau}(r_{12}) v^{bj\tau}(r_{12}) \\ & \times f^{tk\tau}(r_{12}) h^c(\mathbf{r}_1, \mathbf{r}_2) \{ \rho^c(\mathbf{r}_1) \rho^c(\mathbf{r}_2) K^{i\tau j k \tau A k \tau} \\ & - 8 [N_{cc}^c(\mathbf{r}_1, \mathbf{r}_2) - \rho_0(\mathbf{r}_1, \mathbf{r}_2)]^2 K^{i\tau j l \tau} \\ & \times K^{l k \tau m \tau A m \tau} \Delta^{m\tau} C_d(\mathbf{r}_1) C_d(\mathbf{r}_2) \}. \end{aligned} \quad (23)$$

In the above equation a sum over repeated indexes is understood, $(i_\tau, j_\tau, k_\tau, l_\tau, m_\tau = c, \tau)$, the coefficients K^{ijk} , A^i , and Δ^i are given in Ref. [19], and the other FHNC functions are defined in Ref. [24].

For the ^{16}O nucleus, we could check the reliability of this approximation against some CMC results [31]. Using a nuclear matter correlation and the $A14$ potential, we find $\langle v^{b+b\tau} \rangle_{W_0}/A = 0.56$ MeV whereas CMC, with the same correlation, gives an extrapolated value of 0.62 MeV. We did

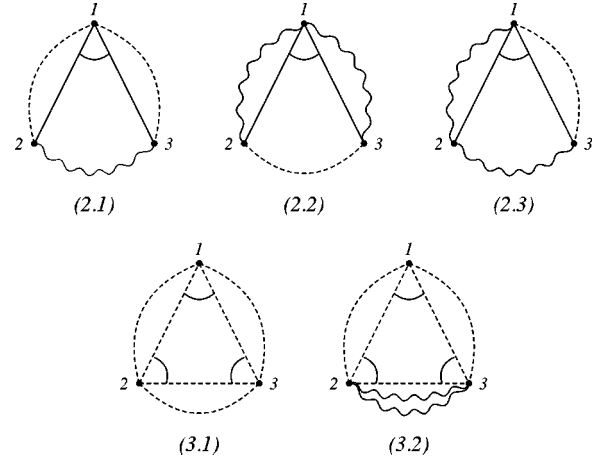


FIG. 1. Cluster diagrams considered for the three-body force expectation value. The 2.1–3 diagrams are related to the $\langle v_{ijk}^{2\pi} \rangle$ part of the force and the 3.1–2 diagrams are related to $\langle v_{ijk}^R \rangle$. The points denote the particle coordinates. The dashed, wavy, and double-wavy lines denote generalized scalar, operator and single-operator ring correlation bonds, respectively. See Ref. [28] for more details.

not find the same kind of agreement for a f_8 correlation, where the W_0 result is -1.23 MeV and CMC gives 0.03 MeV. This supports our choice in favor of the use of a simpler f_6 correlation.

B. Three-body potential

The evaluation of the mean value of the three-body interaction, $\langle v_{ijk} \rangle = \langle v_{ijk}^{2\pi} \rangle + \langle v_{ijk}^R \rangle$, closely follows the method developed in Ref. [28] for nuclear matter. Diagrams 2.1–3 of the reference were shown to provide the relevant contributions to $\langle v_{ijk}^{2\pi} \rangle$, and diagrams 3.1 and 3.2 to $\langle v_{ijk}^R \rangle$. These diagrams, which we show in Fig. 1, are those considered in our calculations.

As an example, we show here how the nuclear matter expression of diagram 2.1 is extended to our case. The explicit expressions for the remaining terms are given in the Appendix.

In diagram 2.1 the pairs of nucleon connected by the operators X_{ij} (pairs 12 and 13 in the figure) are dressed at all orders by Jastrow correlations, whereas the remaining pair (23) bears the full operatorial correlations. Only the anticommutator part of $v_{ijk}^{2\pi}$ contributes to $\langle v_{ijk}^{2\pi} \rangle_{2.1}$. Spin-isospin trace and spatial integration over nucleon 1 generate an effective two-body potential, acting on the 23 pair, having $\sigma\tau$ and $t\tau$ components only and depending on the exchange patterns (xy) of particles 2 and 3,

$$v_{xy}^{eff}(\mathbf{r}_2, \mathbf{r}_3) = \sum_{k=\sigma\tau, t\tau} v_{xy}^{eff.k}(\mathbf{r}_2, \mathbf{r}_3) O_{23}^k, \quad (24)$$

with

$$\begin{aligned}
v_{xy}^{eff,k}(\mathbf{r}_2, \mathbf{r}_3) = & 4A_{2\pi} \int d^3 r_1 \\
& \times \left[\sum_{x'y'} g_{xx'}^c(\mathbf{r}_2, \mathbf{r}_1) V_{x'y'}^c(\mathbf{r}_1) g_{y'y}^c(\mathbf{r}_1, \mathbf{r}_3) \right] \\
& \times \xi_{213}^{i\sigma j\sigma k\sigma} X^{i\sigma}(r_{21}) X^{j\sigma}(r_{13}), \quad (25)
\end{aligned}$$

where $k = k_\sigma \tau$, ($i_\sigma, j_\sigma, k_\sigma = c, \sigma, t$), g_{xy}^c and V_{xy}^c are central partial distribution functions and vertex corrections defined in Ref. [24], ξ_{213}^{ijk} are angular couplings given in Ref. [19], and $X^c(r) = 0$, $X^\sigma(r) = Y(r)$, and $X^t(r) = T(r)$. The allowed combinations for ($x'y'$) are: dd , de , ed , and cc . In the last case also (xy) should be (cc).

The full expression for the mean value of the 2.1 diagram, $\langle v_{ijk}^{2\pi} \rangle_{2.1}$, is then given by

$$\begin{aligned}
\langle v_{ijk}^{2\pi} \rangle_{2.1} = & \frac{1}{2} \int d^3 r_2 \int d^3 r_3 f^i(r_{23}) f^j(r_{23}) h^c(\mathbf{r}_2, \mathbf{r}_3) K^{ikj} A^j \{ v_{dd}^{eff,k}(\mathbf{r}_2, \mathbf{r}_3) [\rho_1^c(\mathbf{r}_2) \rho_1^c(\mathbf{r}_3) + \rho_1^c(\mathbf{r}_2) N_{de}^c(\mathbf{r}_2, \mathbf{r}_3) C_d(\mathbf{r}_3) \\
& + C_d(\mathbf{r}_2) N_{ed}^c(\mathbf{r}_2, \mathbf{r}_3) \rho_1^c(\mathbf{r}_3) + C_d(\mathbf{r}_2) [N_{de}^c(\mathbf{r}_2, \mathbf{r}_3) N_{ed}^c(\mathbf{r}_2, \mathbf{r}_3) + N_{ee}^c(\mathbf{r}_2, \mathbf{r}_3)] C_d(\mathbf{r}_3) \} + v_{de}^{eff,k}(\mathbf{r}_2, \mathbf{r}_3) [\rho_1^c(\mathbf{r}_2) \\
& + C_d(\mathbf{r}_2) N_{ed}^c(\mathbf{r}_2, \mathbf{r}_3)] C_d(\mathbf{r}_3) + v_{ed}^{eff,k}(\mathbf{r}_2, \mathbf{r}_3) C_d(\mathbf{r}_2) [\rho_1^c(\mathbf{r}_3) + N_{de}^c(\mathbf{r}_2, \mathbf{r}_3) C_d(\mathbf{r}_3)] + v_{ee}^{eff,k}(\mathbf{r}_2, \mathbf{r}_3) C_d(\mathbf{r}_2) C_d(\mathbf{r}_3) \} \\
& - 2 \int d^3 r_2 \int d^3 r_3 f^i(r_{23}) f^j(r_{23}) h^c(\mathbf{r}_2, \mathbf{r}_3) C_d(\mathbf{r}_2) C_d(\mathbf{r}_3) K^{ikl} K^{ljm} A^m \Delta^m \{ v_{dd}^{eff,k}(\mathbf{r}_2, \mathbf{r}_3) [N_{cc}^c(\mathbf{r}_2, \mathbf{r}_3) - \rho_0(\mathbf{r}_2, \mathbf{r}_3)]^2 \\
& + 2v_{cc}^{eff,k}(\mathbf{r}_2, \mathbf{r}_3) [N_{cc}^c(\mathbf{r}_2, \mathbf{r}_3) - \rho_0(\mathbf{r}_2, \mathbf{r}_3)] \}. \quad (26)
\end{aligned}$$

Both commutator and anticommutator contributions are present in $\langle v_{ijk}^{2\pi} \rangle_{2.2}$, while only the commutator part contributes to $\langle v_{ijk}^{2\pi} \rangle_{2.3}$.

In Table I we compare the TNI mean values for ^{16}O calculated by FHNC/SOC with the Monte Carlo estimates [31] obtained with the same wave function. We have used the Urbana V three-nucleon interaction [28] and the v_6 truncation of the Urbana v_{14} NN interaction. The correlations have been obtained by the two-body Euler equation and we used harmonic oscillator single particle states with $b = 1.54$ fm. The ^{40}Ca results are also shown.

For the Jastrow correlation the Monte Carlo results have been obtained with a VMC calculation, while for the f_6 correlation the calculation is of the CMC type. In ^{16}O the FHNC/SOC results are in satisfactory agreement with the Monte Carlo ones for both the classes of correlations. The ^{40}Ca results may be compared with those in nuclear matter, where, at saturation density, the Urbana V model gives $\langle v_{ijk}^{2\pi} \rangle = -2.32$ MeV and $\langle v_{ijk}^R \rangle = 3.35$ MeV [28]. The change of sign of $\langle v_{ijk}^{2\pi} \rangle$ between the Jastrow and the operatorial correlation is due to the fact that the attractive contribution comes most from the tensor component of the effective potential, $v_{xy}^{eff,t\tau}(\mathbf{r}_2, \mathbf{r}_3)$, which does not contribute in absence of tensor correlations.

IV. RESULTS

The results presented in this section have been obtained with v_8 type NN interactions, either by truncating the $A14$ potential [25] or by using the $A8'$ potential of Ref. [3], together with f_6 correlations and Urbana three-nucleon potentials. We have estimated the $f^{p>6}$ corrections, as well as the contributions from the $p > 8$ components of the potential, by local density approximation (LDA). In practice, if we define

as $\Delta E_{nm}(\rho)$ the sum of these corrections in nuclear matter at density ρ , we evaluate their contribution in the finite nucleus as

$$\Delta E = \frac{1}{A} \int d^3 r \rho_1(\mathbf{r}) \Delta E_{nm}[\rho_1(\mathbf{r})]. \quad (27)$$

We have already studied the accuracy of FHNC/SOC computational scheme against the results of CMC in Ref. [24]. In the present article we compare again the ^{16}O results with those of CMC in order to test the accuracy in the calculation of the interaction terms we have added. For this reason we have computed the ground state energy for the $A14 + \text{UVII}$ model using a f_6 correlation derived from the nuclear matter two-body Euler equations. The parameters of

TABLE I. TNI expectation values per nucleon, in MeV, in ^{16}O and ^{40}Ca for the Urbana V model. The $f_{1(6)}$ column gives the energies for the Jastrow (operatorial) correlation. The superscript $C(A)$ indicates the commutator (anticommutator) contribution.

	$f_1(\text{FHNC})$	$f_1(\text{VMC})$	$f_6(\text{SOC})$	$f_6(\text{CMC})$
^{16}O				
$\langle v_{ijk}^{2\pi,C} \rangle$	-0.17	-0.16	-0.90	-0.86
$\langle v_{ijk}^{2\pi,A} \rangle$	0.74	0.70	-0.39	-0.44
$\langle v_{ijk}^R \rangle$	1.33	1.28	1.65	1.57
^{40}Ca				
$\langle v_{ijk}^{2\pi,C} \rangle$	-0.24		-1.50	
$\langle v_{ijk}^{2\pi,A} \rangle$	1.80		-0.26	
$\langle v_{ijk}^R \rangle$	2.75		3.20	

TABLE II. FHNC/SOC and CMC energies in MeV/nucleon for ^{16}O with the $A14+UVII$ interaction and the CMC single particle potential and nuclear matter correlation. rms in fm; see text.

	FHNC/SOC	CMC
$\langle T \rangle - T_{cm}$	37.23	32.0
$\langle v_{6,ij} \rangle$	-42.48	-38.2
$\langle v_{7-8,ij} \rangle$	-0.85	
$\langle v_{ijk}^{2\pi} \rangle$	-2.83	
$\langle v_{ijk}^R \rangle$	1.90	
$\langle v_{ijk} \rangle$	-0.93	-1.1
$\langle v_{Coul} \rangle$	1.00	0.9
ΔE	0.05	
ΔE_{CMC}		-0.5
E_{gs}	-5.97	-6.9
rms	2.44	2.43

the correlation are: the Fermi momentum k_F , and the healing distances d_c , used for all the central channels, and d_t for the tensor channels. Additional variational parameters are the quenching factors β_p of the potential (see Eq. (3.2) of Ref. [19]), and as in Ref. [24] we have taken $\beta_1 = 1$ and $\beta_{p>1} = \alpha_S$. We have used the same set of single particle states, produced by a Woods-Saxon (WS) plus wine-bottle mean field potential, and correlation parameters of Ref. [17]. However, small differences in the correlation come on account of the fact that our nuclear matter Euler equation does not contain the $v^{p>6}$ components, contrary to Ref. [17].

The results of these calculations are shown in Table II. The table gives also the corresponding CMC results, as extracted from the reference, by subtracting, when reported, the three-body and spin-orbit correlations contributions. The ΔE_{CMC} line gives the CMC corrections coming from $(f, v)^{p>6}$ and should be compared with the $\Delta E + \langle v_{7-8,ij} \rangle$ sum (-0.5 vs -0.80 MeV/nucleon) in the FHNC/SOC column. The ground state energy E_{gs} is given by $E_{gs} = E_v - T_{cm}$, where T_{cm} is the center of mass kinetic energy. The Coulomb potential energy $\langle v_{Coul} \rangle$ has been included in E_{gs} . The root mean square radii rms are also reported.

The energy found in CMC is -7.7 MeV/nucleon, and it contains a -0.85 MeV/nucleon contribution from explicit three-body correlations. Therefore the FHNC/SOC result (-5.97 MeV/nucleon) should be compared with an estimated CMC value of -6.85 MeV/nucleon. If the CMC ex-

pansion has reached a satisfactory convergence, the discrepancies between the two calculations are due to the truncation in the FHNC/SOC scheme and to the aforementioned differences in the correlation. As it was found in Ref. [24], the FHNC ground state energy differs from the CMC estimate by ~ 1 MeV/nucleon, compatible with the estimated accuracy of the method in nuclear matter. In this calculation the ΔE corrections are small, somehow justifying *a posteriori* the use of LDA. It is remarkable that in the coupled cluster approach of Ref. [32] the authors find $E_{gs}(\text{CC}) = -6.1$ MeV/nucleon with the two-body $A14$ model, close to our estimated $E_{gs}(\text{FHNC/SOC}) = -6.04$ MeV/nucleon (obtained without $\langle v_{ijk} \rangle$ and $\langle v_{Coul} \rangle$).

The nuclear matter energies per nucleon calculated with several interactions are given in Table III as a function of the density. The $A18+UIX$ ($A18$) and $A8'+UIX$ ($A8'$) interactions provide energy minima at the empirical value of the saturation density. The results of the $A18$ column differ from those of Ref. [5] because we have subtracted a perturbative correction, related to additional state dependence of the correlation. The second column of the table shows the results for the $A8'+UIX$ interaction with a f_8 correlation. The contribution of the $f^{p>6}$ terms is given in the third column. For completeness, we also give the results obtained with the full $A14$ potential plus the $UVII$ three-body force and the corresponding $\Delta E/A$. The $A14+UVII$ ($A14$) minimum of the equation of state is located at a density slightly higher than the empirical one.

The ground state energies of ^{16}O and ^{40}Ca calculated with the $A8'+UIX$ and the truncated $A14+UVII$ interactions are shown in Table IV. We have adopted the nuclear matter f_6 correlation, where the nuclear matter density is used as a variational parameter (it means that, for a given ρ_{nm} , we use the correlation function parameters minimizing the nuclear matter energy at that density). In addition, the energy has been minimized over the single particle potential (harmonic oscillator, HO, or WS) parameters. The table also contains the kinetic energies computed with only the mean field wave functions. They are about half of the total kinetic energies obtained in the full calculations and this difference has to be ascribed to the correlations. This type of behavior is also found in nuclear matter. For example, at saturation density and with the $A18+UIX$ Hamiltonian, the nuclear matter calculations of Ref. [5] provide a total kinetic energy of 42.27 MeV/nucleon to be compared with the correspond-

TABLE III. Nuclear matter energies per nucleon for $A18+UIX$ ($A18$), $A8'+UIX$ ($A8'$), and $A14+UVII$ ($A14$). The $\Delta E/A$ columns list the spin-orbit correlation and the $p>8$ potential components corrections. Densities in fm^{-3} , energies in MeV.

ρ_{nm}	E/A ($A18$)	E/A ($A8'$)	$\Delta E/A$ ($A8'$)	E/A ($A14$)	$\Delta E/A$ ($A14$)
0.04	-4.11	-5.50	-0.30	-5.25	-0.80
0.08	-7.46	-8.45	-0.82	-8.43	-0.38
0.12	-9.42	-10.31	-1.48	-10.63	0.00
0.16	-10.05	-10.87	-2.16	-11.99	0.61
0.20	-8.74	-10.06	-3.02	-12.37	0.27
0.24	-5.66	-7.75	-3.96	-11.74	0.50

TABLE IV. Energies in MeV/nucleon for ^{16}O and ^{40}Ca obtained with $A8' + \text{UIX} + f_{6,nn}$ and with truncated $A14 + \text{UVII} + f_{6,nn}$. In the upper part of the table we show the values the minimization parameters. b_{HO} , a_0 , R_0 , are expressed in fm, ρ_{nm} in fm^{-3} all the other quantities in MeV/nucleon. The energy experimental values are -7.97 MeV/nucleon for ^{16}O and -8.55 MeV/nucleon for ^{40}Ca . The experimental rms radii are 2.73 and 3.48 fm for ^{16}O and ^{40}Ca , respectively.

	$^{16}\text{O}(\text{HO})_{A8'}$	$^{16}\text{O}(\text{WS})_{A8'}$	$^{16}\text{O}(\text{WS})_{A14}$	$^{40}\text{Ca}(\text{HO})_{A8'}$	$^{40}\text{Ca}(\text{WS})_{A8'}$	$^{40}\text{Ca}(\text{WS})_{A14}$
b_{HO}	2.00			2.10		
V_0		-42.00	-36.00		-50.00	-41.50
R_0		3.60	3.80		5.30	5.00
a_0		0.55	0.55		0.53	0.55
ρ_{nm}	0.09	0.09	0.09	0.09	0.09	0.09
$\langle T \rangle$	22.57	27.34	25.91	30.02	30.58	30.90
$\langle T \rangle_{IPM}$	11.64	13.82	12.20	14.09	14.15	14.10
$\langle v_{8,ij} \rangle$	-27.49	-32.48	-31.05	-38.03	-38.68	-39.08
$\langle v_{ijk}^{2\pi} \rangle$	-1.15	-1.66	-1.35	-1.94	-1.94	-1.74
$\langle v_{ijk}^R \rangle$	1.26	1.98	1.56	2.46	2.37	2.11
E_{cm}	0.48	0.58	0.52	0.18	0.20	0.19
$\langle v_{Coul} \rangle$	0.78	0.86	0.84	1.85	1.85	1.87
ΔE	-0.66	-0.94	-0.50	-0.95	-0.96	-0.70
E_{gs}	-5.18	-5.48	-5.11	-6.77	-6.97	-6.50
rms	3.03	2.83	2.93	3.65	3.66	3.66

ing Fermi gas value of 22.11 MeV/nucleon. As expected, the minimization with the WS potentials produces lower minima than those obtained with HO potentials. The comparison between the WS calculations done with the two different interactions shows small differences in the results, of the order of 7% in E_{gs} . From the relative point of view the largest differences are those related to ΔE , which for A14 are 50% smaller than those of A8'. These rather similar values of the energies have been obtained with two quite different sets of single particle wave functions. This can be deduced by looking at the values of the WS parameters in Table IV, and even better from Fig. 2 where the FHNC/SOC charge distributions are compared with the independent-particle model (IPM) ones and with the empirical densities taken from the compilation of Ref. [33]. The charge densities have been obtained by folding the proton densities with the electromagnetic form factors of Ref. [34].

We do not obtain a satisfactory agreement between the computed densities and the empirical ones. However, we remark that, for a given type of single particle wave functions, either HO or WS, we find shallow energy minima with respect to variations of the mean field parameters around the minimum itself. This may indicate that charge distributions and rms radii are sensitive to details of the many body wave function which have small effects on the energy calculation. To better study this aspect, we have done calculations by using a set of single particle wave functions fixed to reproduce at best the empirical charge densities. In this case, the only variational parameters are those related to the correlation functions. Actually, we have varied only d_t and kept fixed its ratio with d_c . The results of these calculations with the A8' + UIX interaction are shown in Table V and in Fig. 3. We observe that a large change in the single particle wave functions produces small variations in the energy values,

1.3% in ^{16}O and 4.8% in ^{40}Ca , within the accuracy of the FHNC/SOC scheme. The analysis of these results shows that the values of the kinetic and potential energies have considerably changed, while their sum remains almost constant. The agreement with the empirical densities has clearly improved, as one can also see in Fig. 4 where the elastic electron scattering cross sections calculated in distorted wave Born approximation [35] with the FHNC/SOC charge densities are compared with the experimental data [36]. The best

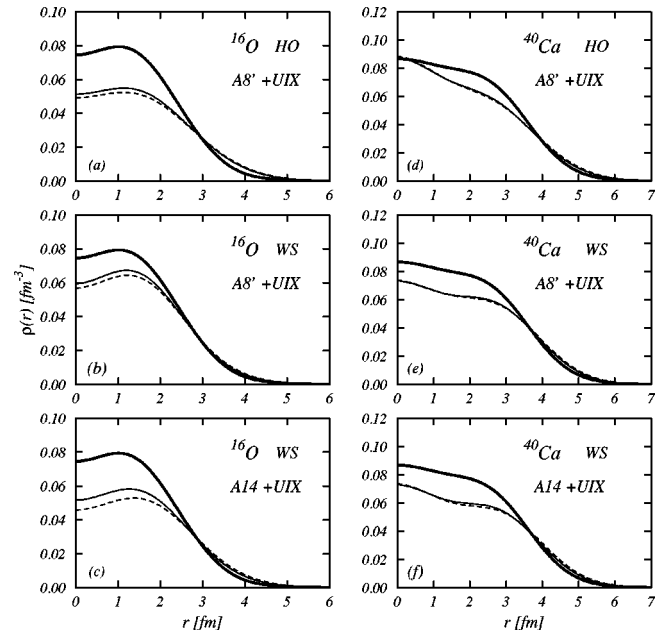


FIG. 2. FHNC/SOC charge densities related to the results of Table IV (thin full lines) compared with the IPM densities (dashed lines) and with the empirical ones (thick full lines).

TABLE V. Energies in MeV/nucleon for ^{16}O and ^{40}Ca obtained with $A8' + \text{UIX} + f_{6,nnm}$ and with WS mean field potentials fixed to reproduce the empirical charge densities. R_0 and a_0 are expressed in fm, ρ_{nm} in fm^{-3} , and the other quantities in MeV/nucleon.

	$^{16}\text{O}(\text{WS})_{A8'}$	$^{40}\text{Ca}(\text{WS})_{A8'}$
V_0	-53.00	-50.00
R_0	3.45	4.60
a_0	0.7	0.5
ρ_{nm}	0.09	0.09
$\langle T \rangle$	32.64	38.15
$\langle T \rangle_{\text{IPM}}$	15.35	16.82
$\langle v_{8,ij} \rangle$	-37.79	-46.34
$\langle v_{ijk}^{2\pi} \rangle$	-2.36	-2.98
$\langle v_{ijk}^R \rangle$	3.00	3.94
E_{cm}	0.64	0.23
$\langle v_{Coul} \rangle$	0.94	2.10
ΔE	-1.21	-1.28
E_{gs}	-5.41	-6.64
rms	2.67	3.39

agreement with the data is produced by the densities of Fig. 3. However, also in this case the high momentum and large energy data are not well described in both nuclei.

From the comparison between the dashed and the thin full lines in Figs. 2 and 3 we can inspect the effects of the correlation on the charge densities. In ^{16}O the correlations enhance the densities with respect to the IPM ones without substantially changing the shape of the oscillation. The effect of the correlations on the ^{40}Ca densities is negligible. These

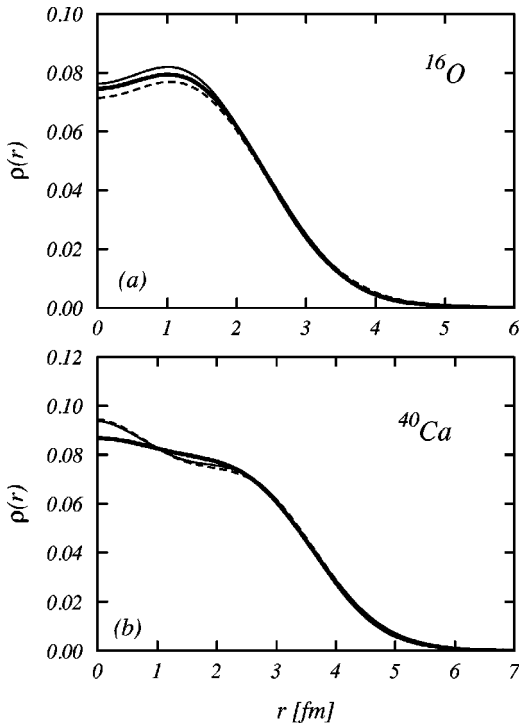


FIG. 3. The same as Fig. 2 for the calculation of Table V.

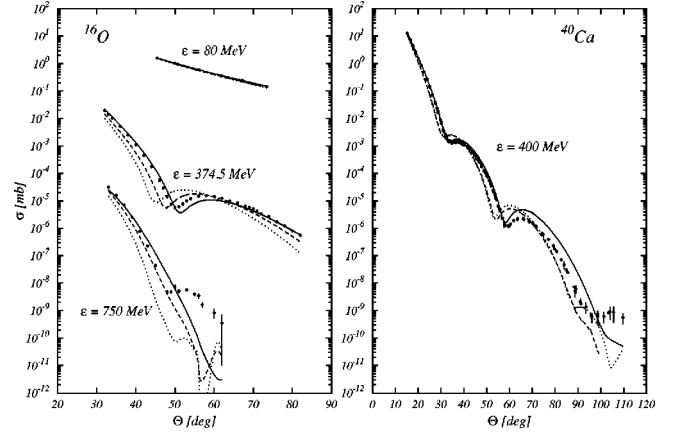


FIG. 4. Electron scattering elastic cross sections for ^{16}O (left) and ^{40}Ca (right). The full lines have been produced by the FHNC/SOC densities of Fig. 3. The other two lines by the WS FHNC/SOC densities of Fig. 2. The dashed lines correspond to the $A8'$ densities while the dotted lines to the $A14$ ones.

results confirm the findings of Ref. [37] where the charge densities have been calculated up to the first order in the correlation lines. On the other hand, in Ref. [17] the correlations produce much larger deviations from the IPM densities. The reason of the different effect of the correlations on the densities of ^{40}Ca and ^{16}O is presently object of investigation.

Short range correlations strongly affect the two-body densities (18). Their effect is evident in the two-nucleon distribution function $\rho_2(r_{12})$ defined as

$$\rho_2(r_{12}) = \frac{1}{A} \int d^3R_{12} \rho_2^c(\mathbf{r}_1, \mathbf{r}_2), \quad (28)$$

where $\mathbf{R}_{12} = \frac{1}{2}(\mathbf{r}_1 + \mathbf{r}_2)$ is the center of mass coordinate. In an analogous way, we define the proton-proton distribution function $\rho_{pp}(r_{12})$ as

$$\rho_{pp}(r_{12}) = \frac{1}{Z} \int d^3R_{12} \rho_{pp}(\mathbf{r}_1, \mathbf{r}_2), \quad (29)$$

where the pp -two-body density is

$$\begin{aligned} \rho_{pp}(\mathbf{r}_1, \mathbf{r}_2) &= \left\langle \sum_{i \neq j} \delta(\mathbf{r}_1 - \mathbf{r}_i) \delta(\mathbf{r}_2 - \mathbf{r}_j) \left(\frac{1 + \tau_{i,z}}{2} \right) \left(\frac{1 + \tau_{j,z}}{2} \right) \right\rangle \\ &= \frac{1}{4} \rho_2^c(\mathbf{r}_1, \mathbf{r}_2) + \frac{1}{12} \rho_2^{\bar{c}}(\mathbf{r}_1, \mathbf{r}_2). \end{aligned} \quad (30)$$

Figure 5 shows $\rho_2(r_{12})$ and $\rho_{pp}(r_{12})$ with the wave functions of Table V, compared with the IPM densities. The reduction of the correlated distribution functions at small r_{12} values is due to the repulsive core of the interaction. We have calculated the FHNC/SOC ^{16}O distribution functions also for the $A14 + \text{UVII}$ model and we found that they are rather similar to the $A8' + \text{UIX}$ ones [$\rho_2^{\text{max}}(A14 + \text{UVII}) \sim 0.081$, $\rho_2^{\text{max}}(A8' + \text{UIX}) \sim 0.089$, $\rho_{pp}^{\text{max}}(A14 + \text{UVII})$

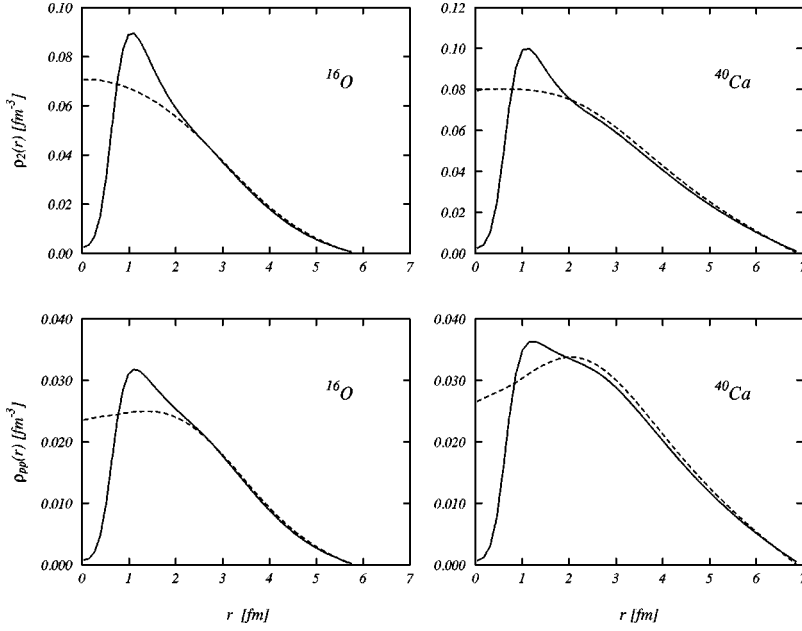


FIG. 5. Two-nucleon (upper panels) and proton-proton (lower panels) distribution functions for the $A8' + \text{UIX}$ interaction. The dashed lines give the IPM results, the solid lines the FHNC/SOC ones.

~ 0.032 , and $\rho_{pp}^{max}(A8' + \text{UIX}) \sim 0.032$], and in good agreement with those computed in Ref. [17].

The interest in calculating the two-body densities is also related to the possibility of using their Fourier transforms to analyze several integrated nuclear responses. The responses of the nucleus to external probes, either of electromagnetic or hadronic type, can be related to the dynamical structure functions $S_X(q, \omega)$ given by

$$S_X(q, \omega) = \sum_I |\langle \Psi_I | O_X | \Psi_0 \rangle|^2 \delta(\omega_I - \omega_0 - \omega), \quad (31)$$

where O_X is the operator producing the fluctuations around the ground state Ψ_0 . In the above equation the sum runs over the intermediate Ψ_I states with energy ω_I . The nonenergy weighted sums of $S_X(q, \omega)$ give the static structure functions (or, simply, structure functions, SF), $S_X(q)$, as

$$S_X(q) = \int S_X(q, \omega) d\omega = \langle \Psi_0 | O_X^\dagger O_X | \Psi_0 \rangle. \quad (32)$$

In the case of density fluctuations, the operator is

$$\rho_{\mathbf{q}} = \sum_{i=1,A} \exp(i\mathbf{q} \cdot \mathbf{r}_i) \quad (33)$$

and the lower limit ω integration in Eq. (32) is taken in an appropriate way to eliminate the contribution of the elastic scattering. The density SF, $S(q)$, is then

$$S(q) = 1 + \frac{1}{A} \int d^3r_1 d^3r_2 \exp(i\mathbf{q} \cdot \mathbf{r}_{12}) \{ \rho_2^c(\mathbf{r}_1, \mathbf{r}_2) - \rho_1(\mathbf{r}_1) \rho_1(\mathbf{r}_2) \}. \quad (34)$$

From the normalizations of the one- and two-body densities, one obtains $S(q=0) = 0$.

The response to charge fluctuations is driven by the operator

$$\rho_{c,\mathbf{q}} = \sum_{i=1,A} \exp(i\mathbf{q} \cdot \mathbf{r}_i) \left(\frac{1 + \tau_{i,z}}{2} \right), \quad (35)$$

which is responsible also of the electromagnetic longitudinal response, if the small ($\sim 2\%$) contributions of the neutron magnetic moment and of the meson-exchange currents are disregarded. The longitudinal response is measured in inelastic electron-nucleus experiments and its energy integral gives the longitudinal SF, $S_L(q)$, or Coulomb sum. In the nuclei we are studying, the explicit expression of $S_L(q)$ reads

$$S_L(q) = 1 + \frac{1}{4Z} \int d^3r_1 d^3r_2 \exp(i\mathbf{q} \cdot \mathbf{r}_{12}) \times \left\{ \rho_2^c(\mathbf{r}_1, \mathbf{r}_2) + \frac{1}{3} \rho_2^s(\mathbf{r}_1, \mathbf{r}_2) - \rho_1(\mathbf{r}_1) \rho_1(\mathbf{r}_2) \right\}. \quad (36)$$

In Fig. 6 we present the density (upper panel) and charge (lower panel) SF for ^{16}O , calculated with the wave functions of Table V. The FHNC/SOC results obtained from our calculations are shown by the white triangles. The $q=0$ value is very sensitive even to small violations of the normalizations of the densities. For instance, the two-body density normalization of Eq. (20), with the Table V parameters, is violated in ^{16}O by only 5.3% and that of the one-body density, Eq. (19), by 2.0%. These acceptable normalization errors produce the large values $S(q=0) = 1.61$ and $S_L(q=0) = 0.86$.

The SF obtained after properly renormalizing the densities are given in Fig. 6 as full curves. The other curves show the IPM SF (dashed lines) and those obtained with only Jastrow correlations. The renormalization is effective only at small q values and for $q > 1 \text{ fm}^{-1}$ the SF remain unchanged. Analogous calculations done in ^{40}Ca show a similar behavior.

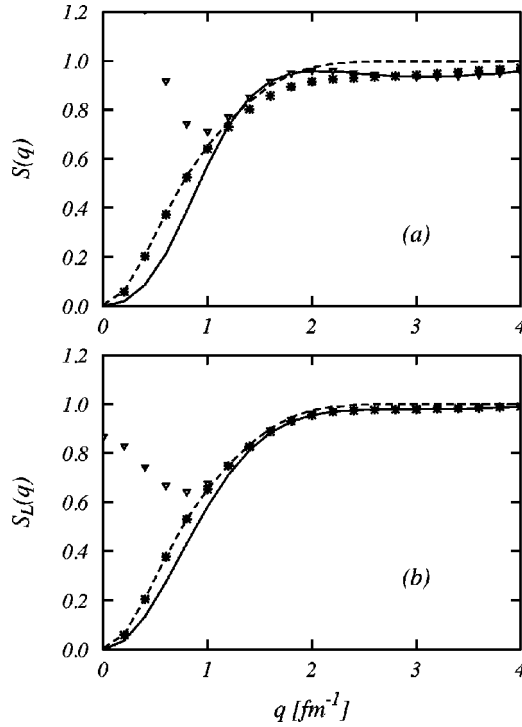


FIG. 6. Density (upper panel) and longitudinal (lower panel) structure functions for ^{16}O (left) for the $A8' + \text{UIX}$ interaction. The IPM (dashed lines), FHNC/SOC (solid lines), non-normalized FHNC/SOC (triangles), and Jastrow (stars) results are given.

ior. Hence the conclusions about the large- q importance of the correlations in the SF and densities are not affected by the normalization problems. In agreement with the findings of Ref. [17], our results show that the correlations, both of the Jastrow and operatorial types, lower the SF at large q .

In Fig. 7 we compare the Coulomb sum rules calculated for ^{16}O and ^{40}Ca with the $A8' + \text{UIX}$ interaction with the experimental estimates done by analyzing the set of world data on inclusive quasielastic electron scattering [38] experiments in ^{12}C , ^{40}Ca , and ^{56}Fe . The figure also shows the nuclear matter Coulomb sum for the $A14 + \text{UVII}$ model from Ref. [39]. The finite nuclei results are in complete agreement with the latest analysis of the experimental data, where a detailed study of the electron scattering world experiments and a proper inclusion of the large energy tail in the dynamical response were carried out. The nuclear matter results fail in reproducing the data at the lowest q values where finite size effects can be still important.

Besides the density and charge SF also the isovector spin longitudinal and transverse (ISL and IST) SF are of experimental interest since they can be extracted from polarized proton and neutron scattering cross section data. Experiments of this type on ^{12}C and ^{40}Ca nuclei [40] did not confirm the prediction of random phase approximation [41] and distorted-wave impulse approximation [42] calculations of a large enhancement, with respect to unity, of the ratio of the ISL to the IST response at small energies.

The ratio has been calculated for nuclear matter within the CBF theory, using a f_6 correlation together with the Urbana $v_{14} + \text{TNI}$ potential [43]. The computed average enhance-

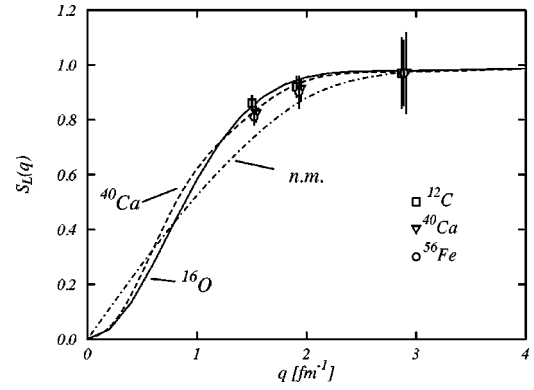


FIG. 7. Coulomb sums for ^{16}O , ^{40}Ca and nuclear matter (*n.m.*) compared with the experimental results from ^{12}C , ^{40}Ca , and ^{56}Fe .

ment was $\sim 20\%$, compatible with the data in heavy nuclei at energies below 100 MeV. However, the nuclear matter calculation did not take into account the strong distortion of the emitted nucleon wave function. Variational and cluster Monte Carlo wave functions were used in Ref. [44] to evaluate the integrated spin responses in light nuclei and ^{16}O . A maximum 25% enhancement of the ratio was found in ^{16}O .

The fluctuation operators in the isovector spin responses are

$$\rho_{\sigma L, \mathbf{q}} = \sum_{i=1, A} \exp(i\mathbf{q} \cdot \mathbf{r}_i) (\sigma_i \cdot \mathbf{q}) (\tau_i \cdot \mathbf{T}) \quad (37)$$

in the longitudinal case, and

$$\rho_{\sigma T, \mathbf{q}} = \sum_{i=1, A} \exp(i\mathbf{q} \cdot \mathbf{r}_i) (\sigma_i \times \mathbf{q}) (\tau_i \cdot \mathbf{T}) \quad (38)$$

in the transverse one. In the above equations we have indicated with \mathbf{T} a unit vector in the isospin space. If the nucleus has zero isospin, then the response does not depend on the direction of \mathbf{T} , except for the small Coulomb effects. Following the treatment of Ref. [44], we obtain for the ISL structure function $S_{\sigma L}(q)$ the expression

$$\begin{aligned} S_{\sigma L}(q) &= \frac{S_{\sigma L}^u(q)}{Aq^2} \\ &= 1 + \frac{1}{9A} \int d^3r_1 d^3r_2 \{ \rho_2^{\sigma\sigma}(\mathbf{r}_1, \mathbf{r}_2) j_0(qr_{12}) \\ &\quad - \rho_2^{\tau\tau}(\mathbf{r}_1, \mathbf{r}_2) j_2(qr_{12}) \}, \end{aligned} \quad (39)$$

and for the IST one, $S_{\sigma T}(q)$,

$$\begin{aligned} S_{\sigma T}(q) &= \frac{S_{\sigma T}^u(q)}{2Aq^2} \\ &= 1 + \frac{1}{9A} \int d^3r_1 d^3r_2 \left\{ \rho_2^{\sigma\sigma}(\mathbf{r}_1, \mathbf{r}_2) j_0(qr_{12}) \right. \\ &\quad \left. + \frac{1}{2} \rho_2^{\tau\tau}(\mathbf{r}_1, \mathbf{r}_2) j_2(qr_{12}) \right\}. \end{aligned} \quad (40)$$

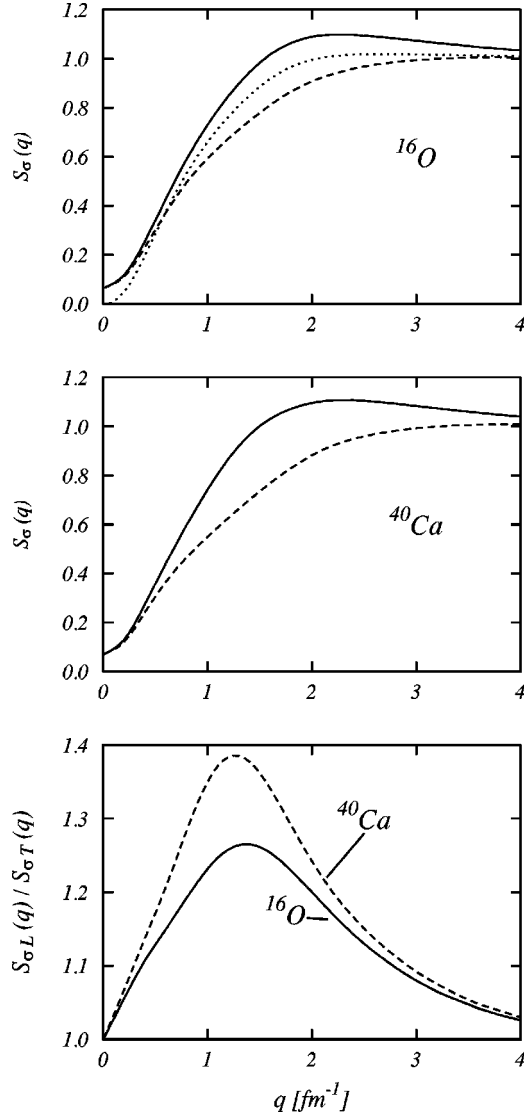


FIG. 8. Isovector spin longitudinal (solid) and transverse (dashed) structure functions for the ^{16}O and ^{40}Ca nuclei. For ^{16}O we show also the Jastrow results (dotted line). The lowest panel gives the ratios of the isovector spin longitudinal and transverse structure functions for both nuclei.

The ISL and IST structure functions for ^{16}O and ^{40}Ca , calculated with the wave functions of Table V, are shown in Fig. 8 as a function of the momentum transfer. For the ^{16}O nucleus we show also the Jastrow results, identical for both ISL and IST. Central correlations do not differentiate between the longitudinal and transverse responses because of the lack of tensor correlations. Our ^{16}O results are very close to those of Ref. [44] obtained with the A14+UVII interaction. The lowest panel of Fig. 8 shows the $S_{\sigma L}(q)/S_{\sigma T}(q)$ ratio. We observe that the maximum enhancement is $\sim 25\%$ in ^{16}O and $\sim 38\%$ in ^{40}Ca , close to the experimental value.

V. CONCLUSIONS

This paper is the natural extension of the work of Ref. [24]. We have added to the FHNC/SOC computational

scheme for doubly closed shell nuclei in ls coupling, the contribution of the spin-orbit and three-body interactions. Our calculations of ^{16}O and ^{40}Ca nuclei have been done considering a f_6 type of correlation and v_8 potentials: the A8'+UIX [3] and a truncated version of the A14+UVII [25] potentials. The contribution from the remaining momentum dependent terms of the correlation and of the potential are estimated by means of a local density interpolation of their nuclear matter values.

The main results of the paper are given in Tables IV and V where the ^{16}O and ^{40}Ca ground state energies per nucleon are presented. Their values are $\sim 2-3$ MeV/nucleon above the experimental ones, consistently with the CBF results in nuclear matter. Additional lowering of the energies may be obtained by (i) three-body correlations, and (ii) perturbative corrections to the two-body correlations. It has been already mentioned that three-body correlations have been found to provide an extra 0.8 MeV/nucleon binding in ^{16}O for the A14+UVII model. Perturbative corrections have been taken into account in nuclear matter either by the method discussed in Ref. [5] or by the inclusion of the second order two-particle two-hole contribution in correlated basis perturbation theory [45,46]. Both approaches lower the energy by $\Delta E_2 \sim 2$ MeV/nucleon. The nuclear matter case gives a strong indication that the inclusion of these corrections should be pursued and that their quantitative consistency in finite nuclear systems needs to be numerically checked.

A complete minimization over all the parameters of the wave functions, both in the correlation and in the mean field, has led to a marked disagreement between the CBF and the empirical charge densities in the low distance region. However, calculations with different sets of single particle wave functions, reproducing the empirical densities in IPM, provided energies differing from the best minima only by a few percent. The CBF scheme does not appear to be very sensitive to the details of the mean field basis in a parameters region around the variational minimum. Nevertheless, these details become relevant for a correct description of the one- and two-body densities. The introduction of additional constraints during the minimization process may be necessary in order to avoid these ambiguities.

Our results show that the short-range correlations produce small effects on the charge density distributions, especially in ^{40}Ca where the FHNC scheme is supposed to perform better. These findings are in agreement with those of Ref. [37] where the same kind of nuclear matter correlations have been used. The sensitivity of the charge distributions to the state dependent short-range correlations requires further investigations to be fully clarified. In effect, the VMC one body densities of [17] have larger dependence on these components.

In addition to the ground state energies, we have studied the static structure functions. The FHNC results for the Coulomb sum rule fully agree with the empirical values. The ratio between the ISL and IST SF shows an enhancement between 25% in ^{16}O and 38% in ^{40}Ca , in agreement with those of Refs. [43] and [44] and just slightly higher than the experimental estimates.

From this work we can conclude that realistic variational

calculations for medium-heavy, doubly closed shell nuclei in ls coupling scheme with modern, sophisticated potentials are not only feasible, but have also reached the same degree of accuracy as in nuclear matter.

There are several natural extensions we envisage. For instance, the inclusion of three-body correlations, the study of $N \neq Z$ closed shell nuclei and the development of the FHNC/SOC formalism for the jj coupling scheme. Work along these directions is in progress.

ACKNOWLEDGMENTS

We want to thank Ingo Sick, Juerg Jourdan, and Steven Pieper for providing us with the elastic electron scattering data, the Coulomb sum rule experimental analysis, and the ^{16}O Monte Carlo results, respectively.

APPENDIX

In this Appendix we give the explicit expressions of the remaining diagrams contributing to the three-nucleon potential expectation value in FHNC/SOC:

$$\begin{aligned} \langle v_{ijk}^{2\pi} \rangle_{2,2} &= 6A_{2\pi} \int d^3r_1 \int d^3r_2 \int d^3r_3 \frac{f^{i\sigma\tau}(r_{12})}{f^c(r_{12})} \\ &\times X^{l\sigma}(r_{12}) \frac{f^{j\sigma\tau}(r_{13})}{f^c(r_{13})} X^{m\sigma}(r_{13}) [R^{i\sigma j\sigma l\sigma m\sigma} \\ &+ 3A^{i\sigma} \delta_{i\sigma l} A^{j\sigma} \delta_{j\sigma m}] \rho_3^c(\mathbf{r}_1, \mathbf{r}_2, \mathbf{r}_3), \quad (\text{A1}) \end{aligned}$$

$$\begin{aligned} \langle v_{ijk}^{2\pi} \rangle_{2,3} &= 12A_{2\pi} \int d^3r_1 \int d^3r_2 \int d^3r_3 \frac{f^{i\sigma\tau}(r_{12})}{f^c(r_{12})} \\ &\times X^{l\sigma}(r_{12}) \frac{f^{j\sigma\tau}(r_{23})}{f^c(r_{23})} X^{m\sigma}(r_{13}) [L^{i\sigma l\sigma n\sigma} \\ &- K^{i\sigma l\sigma n\sigma} A^{n\sigma}] \xi_{231}^{j\sigma m\sigma n\sigma} \rho_3^c(\mathbf{r}_1, \mathbf{r}_2, \mathbf{r}_3), \quad (\text{A2}) \end{aligned}$$

$$\langle v_{ijk}^R \rangle_{3,1} = \frac{1}{6} \int d^3r_1 \int d^3r_2 \int d^3r_3 v_{123}^R \rho_3^c(\mathbf{r}_1, \mathbf{r}_2, \mathbf{r}_3), \quad (\text{A3})$$

$$\begin{aligned} \langle v_{ijk}^R \rangle_{3,2} &= \frac{1}{2} \int d^3r_1 \int d^3r_2 \int d^3r_3 v_{123}^R \\ &\times \frac{f^i(r_{23}) f^k(r_{23})}{[f^c(r_{23})]^2} K^{ikm} A^m [\rho_{3,dir}^c(\mathbf{r}_1, \mathbf{r}_2, \mathbf{r}_3) \delta_{ik} \\ &+ \rho_{3,exch}^c(\mathbf{r}_1, \mathbf{r}_2, \mathbf{r}_3) \Delta^m]. \quad (\text{A4}) \end{aligned}$$

The L^{ijk} and R^{ijkl} matrices are given in Refs. [19] and [28], respectively. The central three-body density, $\rho_3^c(\mathbf{r}_1, \mathbf{r}_2, \mathbf{r}_3)$, is written in superposition approximation as

$$\begin{aligned} \rho_3^c(\mathbf{r}_1, \mathbf{r}_2, \mathbf{r}_3) &= \sum_{xyzx'y'z'=d,e} g_{xx'}^c(\mathbf{r}_1, \mathbf{r}_2) V_{x'y'}^c(\mathbf{r}_2) \\ &\times g_{y'y'}^c(\mathbf{r}_2, \mathbf{r}_3) V_{yz}^c(\mathbf{r}_3) g_{zz'}^c(\mathbf{r}_3, \mathbf{r}_1) V_{z'x}^c(\mathbf{r}_1) \\ &- 8g_{cc}^c(\mathbf{r}_1, \mathbf{r}_2) V_{cc}^c(\mathbf{r}_2) g_{cc}^c(\mathbf{r}_2, \mathbf{r}_3) \\ &\times V_{cc}^c(\mathbf{r}_3) g_{cc}^c(\mathbf{r}_3, \mathbf{r}_1) V_{cc}^c(\mathbf{r}_1). \quad (\text{A5}) \end{aligned}$$

As already stated, only the ee combination is not allowed at a given vertex. The *exchange* and *direct* three-body densities, $\rho_{3,exch/dir}^c(\mathbf{r}_1, \mathbf{r}_2, \mathbf{r}_3)$, are given by those parts of the full density where nucleons 2 and 3 belong or not to the same exchange loop.

-
- [1] C. R. Chen, G. L. Payne, J. L. Friar, and B. F. Gibson, Phys. Rev. C **33**, 1740 (1986); A. Stadler, W. Glöckle, and P. U. Sauer, *ibid.* **44**, 2319 (1991).
- [2] A. Kievsky, M. Viviani, and S. Rosati, Nucl. Phys. **A551**, 241 (1993).
- [3] B. S. Pudliner, V. R. Pandharipande, J. Carlson, S. C. Pieper, and R. B. Wiringa, Phys. Rev. C **56**, 1720 (1997).
- [4] R. B. Wiringa, V. Ficks, and A. Fabrocini, Phys. Rev. C **38**, 1010 (1988).
- [5] A. Akmal, V. R. Pandharipande, and D. G. Ravenhall, Phys. Rev. C **58**, 1804 (1998).
- [6] B. A. Friedman and V. R. Pandharipande, Nucl. Phys. **A361**, 502 (1981).
- [7] A. Akmal and V. R. Pandharipande, Phys. Rev. C **56**, 2261 (1997).
- [8] A. Fabrocini and S. Fantoni, Nucl. Phys. **A503**, 375 (1989).
- [9] A. Fabrocini, Phys. Rev. C **55**, 338 (1997).
- [10] O. Benhar, A. Fabrocini, and S. Fantoni, Nucl. Phys. **A550**, 201 (1992).
- [11] R. A. Arndt, L. D. Roper, R. L. Workman, and M. W. McNaughton, Phys. Rev. D **45**, 3995 (1992).
- [12] V. G. J. Stoks, R. A. M. Klomp, M. C. M. Rentmeester, and J. J. DeSwart, Phys. Rev. C **48**, 792 (1993).
- [13] V. G. J. Stoks, R. A. M. Klomp, C. P. F. Terheggen, and J. J. DeSwart, Phys. Rev. C **49**, 2950 (1994).
- [14] R. B. Wiringa, V. G. J. Stoks, and R. Schiavilla, Phys. Rev. C **51**, 38 (1995).
- [15] R. Machleidt, F. Sammarruca, and Y. Song, Phys. Rev. C **53**, R1483 (1996).
- [16] R. B. Wiringa, Phys. Rev. C **43**, 1585 (1991).
- [17] S. C. Pieper, R. B. Wiringa, and V. R. Pandharipande, Phys. Rev. C **46**, 1741 (1992).
- [18] S. Rosati, in *From Nuclei to Particles*, Proceedings of the International School of Physics "Enrico Fermi," Course LXXIX, Varenna, 1981, edited by A. Molinari (North-Holland, Amsterdam, 1982).

- [19] V. R. Pandharipande and R. B. Wiringa, *Rev. Mod. Phys.* **51**, 821 (1979).
- [20] R. B. Wiringa, *Nucl. Phys.* **A338**, 57 (1980).
- [21] G. Co', A. Fabrocini, S. Fantoni, and I. E. Lagaris, *Nucl. Phys.* **A549**, 439 (1992).
- [22] G. Co', A. Fabrocini, and S. Fantoni, *Nucl. Phys.* **A568**, 73 (1994).
- [23] F. Arias de Saavedra, G. Co', A. Fabrocini, and S. Fantoni, *Nucl. Phys.* **A605**, 359 (1996).
- [24] A. Fabrocini, F. Arias de Saavedra, G. Co', and P. Folgarait, *Phys. Rev. C* **57**, 1668 (1998).
- [25] R. B. Wiringa, R. A. Smith, and T. L. Ainsworth, *Phys. Rev. C* **29**, 1207 (1984).
- [26] R. Schiavilla, V. R. Pandharipande, and R. B. Wiringa, *Nucl. Phys.* **A449**, 219 (1986).
- [27] J. Fujita and H. Miyazawa, *Prog. Theor. Phys.* **17**, 360 (1957).
- [28] J. Carlson, V. R. Pandharipande, and R. B. Wiringa, *Nucl. Phys.* **A401**, 59 (1983).
- [29] I. E. Lagaris and V. R. Pandharipande, *Nucl. Phys.* **A359**, 331 (1981); *ibid.* **A359**, 349 (1981).
- [30] I. E. Lagaris and V. R. Pandharipande, *Nucl. Phys.* **A334**, 217 (1980).
- [31] S. C. Pieper (private communication).
- [32] J. H. Heisenberg and B. Mihaila, *Phys. Rev. C* **59**, 1440 (1999).
- [33] C. W. De Jager and C. De Vries, *At. Data Nucl. Data Tables* **36**, 495 (1987).
- [34] G. Hoehler, E. Pietarinen, I. Sabba-Stefabescu, F. Borkowski, G. G. Simon, V. H. Walther, and R. D. Wendling, *Nucl. Phys.* **B114**, 505 (1976).
- [35] R. Anni, G. Co', and P. Pellegrino, *Nucl. Phys.* **A584**, 35 (1995); R. Anni and G. Co', *ibid.* **A588**, 463 (1995).
- [36] I. Sick and J. S. McCarthy, *Nucl. Phys.* **A150**, 631 (1970); B. B. P. Sinha, G. A. Peterson, R. R. Whitney, I. Sick, and J. S. McCarthy, *Phys. Rev. C* **7**, 1930 (1973); I. Sick, J. Bellicard, J. Cavedon, B. Frois, M. Huet, P. Leconte, P. Ho, and S. Platchkov, *Phys. Lett.* **B88**, 245 (1979); J. Cavedon, Ph.D. thesis, Université de Paris-sud, Paris 1980; I. Sick (private communication).
- [37] F. Arias de Saavedra, G. Co', and M. M. Renis, *Phys. Rev. C* **55**, 673 (1997).
- [38] J. Jourdan, *Nucl. Phys.* **A603**, 117 (1996); (private communication).
- [39] R. Schiavilla, D. S. Lewart, V. R. Pandharipande, S. C. Pieper, and R. B. Wiringa, *Nucl. Phys.* **A473**, 267 (1987).
- [40] J. M. McClelland *et al.*, *Phys. Rev. Lett.* **69**, 582 (1992).
- [41] W. M. Alberico, M. Ericson, and A. Molinari, *Nucl. Phys.* **A379**, 429 (1982).
- [42] M. Ichimura, K. Kawahigashi, T. S. Jorgensen, and C. Garde, *Phys. Rev. C* **39**, 1446 (1989).
- [43] A. Fabrocini, *Phys. Lett. B* **322**, 171 (1994).
- [44] V. R. Pandharipande, J. Carlson, S. C. Pieper, R. B. Wiringa, and R. Schiavilla, *Phys. Rev. C* **49**, 789 (1994).
- [45] S. Fantoni, B. L. Friman, and V. R. Pandharipande, *Nucl. Phys.* **A399**, 57 (1983).
- [46] A. Fabrocini and S. Fantoni, *Phys. Lett. B* **298**, 263 (1993).